Intercomparison of Simulated Global Vegetation Distributions in Response to 6 kyr BP Orbital Forcing

S. P. HARRISON,* D. JOLLY,+ F. LAARIF,* A. ABE-OUCHI,# B. DONG,@ K. HERTERICH,& C. HEWITT,**
S. JOUSSAUME,++,## J. E. KUTZBACH,@@ J. MITCHELL,** N. DE NOBLET,++ AND P. VALDES@

* *Dynamic Palaeoclimatology Group, Lund University, Lund, Sweden*
\+ *Global Systems Group, Department of Ecology, Lund University, Lund, Sweden*
\# *Centre for Climate System Research, University of Tokyo, Tokyo, Japan*
@ *Department of Meteorology, University of Reading, Reading, United Kingdom*
& *Fachbereichs Geowissenschaften Universität Bremen, Bremen, Germany*
** *Hadley Centre for Climate Prediction and Research, Meteorological Office, Bracknell, Berkshire, United Kingdom*
++ *Laboratoire de Modélisation du Climat et Environnement, CEA Saclay, Orme des Merisiers, Gif-sur-Yvette, France*
Laboratoire d'Océanographie Dynamique et de Climatologie, CNRS/ORSTOM/UPMC, Paris, France
@@ *Center for Climatic Research, University of Wisconsin—Madison, Madison, Wisconsin*

(Manuscript received 3 March 1997, in final form 19 August 1997)

ABSTRACT

The response of ten atmospheric general circulation models to orbital forcing at 6 kyr BP has been investigated using the BIOME model, which predicts equilibrium vegetation distribution, as a diagnostic. Several common features emerge: (a) reduced tropical rain forest as a consequence of increased aridity in the equatorial zone, (b) expansion of moisture-demanding vegetation in the Old World subtropics as a consequence of the expansion of the Afro–Asian monsoon, (c) an increase in warm grass/shrub in the Northern Hemisphere continental interiors in response to warming and enhanced aridity, and (d) a northward shift in the tundra–forest boundary in response to a warmer growing season at high northern latitudes. These broadscale features are consistent from model to model, but there are differences in their expression at a regional scale. Vegetation changes associated with monsoon enhancement and high-latitude summer warming are consistent with palaeoenvironmental observations, but the simulated shifts in vegetation belts are too small in both cases. Vegetation changes due to warmer and more arid conditions in the midcontinents of the Northern Hemisphere are consistent with palaeoenvironmental data from North America, but data from Eurasia suggests conditions were wetter at 6 kyr BP than today. The models show quantitatively similar vegetation changes in the intertropical zone, and in the northern and southern extratropics. The small differences among models in the magnitude of the global vegetation response are not related to differences in global or zonal climate averages, but reflect differences in simulated regional features. Regional-scale analyses will therefore be necessary to identify the underlying causes of such differences among models.

1. Introduction

The magnitude of potential future climate changes is substantially larger than the variations experienced during periods for which instrumental observations are available (Kattenberg et al. 1996). The use of directly observed meteorological data is central to the strategy for validation and development of atmospheric general circulation models (AGCMs), but it is also important to test the performance of AGCMs under radically different climate conditions. The recent geological past offers several opportunities when (a) the change in climate forcing was both accurately known and at least as large as that expected due to increasing greenhouse gas concentrations, and (b) there is abundant proxy climate data with which the simulations can be compared (COHMAP Members 1988). Simulations of key times in the past (e.g., the last glacial maximum or the early- or mid-Holocene) have been carried out by several modeling groups independently (e.g., Williams et al. 1974; Gates 1976; Manabe and Hahn 1977; Kutzbach and Otto-Bleisner 1982; Manabe and Broccoli 1985; Kutzbach and Guetter 1986; Rind 1987; Kutzbach and Gallimore 1988; Mitchell et al. 1988; Joussaume et al. 1989; Lautenschlager and Herterich 1990; Kutzbach et al. 1993; Liao et al. 1994; Kutzbach et al. 1998), and have led to increased confidence in the ability of AGCMs to capture the first-order spatial patterns of past climate changes (Wright et al. 1993; Gates et al. 1996). However, these experiments were designed independently by

Corresponding author address: Dr. S. P. Harrison, Max Planck Institute for Biogeochemistry, P.O. Box 100164, D-07701 Jena, Germany.
E-mail: sandy.harrison@bgc-jena.mpg.de

each modeling group (resulting in the use of slightly different boundary conditions for the same time period) so the usefulness of comparing existing simulations is limited.

The potential of palaeoclimate simulations for climate model evaluation is being exploited more systematically by the Palaeoclimate Modelling Intercomparison Project (PMIP). PMIP's goals are to intercompare climate models driven by the same palaeoclimate forcing, in order to better understand the mechanisms of climate change and to test the ability of the models to reproduce climatic conditions radically different from today (Joussaume and Taylor 1995). The project is parallel to the model–model comparisons being carried out for present-day climate [the Atmospheric Model Intercomparison Project (AMIP), see Gates (1992)]. For each PMIP experiment, as in AMIP, the boundary conditions have been precisely specified. Because each modeling group uses exactly the same boundary conditions, differences between the simulations must reflect differences in model structure and parameterizations. Model intercomparisons are then designed (a) to identify similarities and differences in the simulated climates, and (b) to isolate the mechanism(s) responsible for the differences.

In its initial phase, PMIP focused on two time periods: the last glacial maximum (21 kyr BP) to examine the effects of large ice sheets and lowered CO_2 on atmospheric circulation, and 6 kyr BP to examine the effects of changes in the seasonal and latitudinal distribution of insolation. In this paper, we consider results from the 6 kyr BP experiment, which provides an opportunity to examine the effects of insolation forcing due to orbital variations. During the period since the last glacial maximum, the precession of the earth's orbit shifted perihelion from January at 21 kyr BP to July at 11 kyr BP to January today, while the tilt of the earth's axis changed from 22.9° at 21 kyr BP to 24.2° at 11 kyr BP and 23.4° today. These changes systematically altered the seasonal and latitudinal distribution of insolation (Berger 1978; Berger and Loutre 1991; Berger et al. 1993). At the time of the maximum anomaly, ≈11 kyr BP, Northern Hemisphere summer (June–August) radiation at the top of the atmosphere was circa 30 W m^{-2} (~8%) greater and winter (December–February) radiation circa 15 W m^{-2} (~8%) less than present. However, because of the lag in the ice sheets' response to insolation forcing (Imbrie 1985), Northern Hemisphere ice sheets were still more extensive at 11 kyr BP than today (Peltier 1994). The mid-Holocene (6 kyr BP) provides an opportunity to isolate the effects of insolation, because the insolation anomaly was still large (~6% greater in Northern Hemisphere summer and less in Northern Hemisphere winter) but the ice sheets were similar to today's. The choice of 6 kyr BP as a PMIP experiment was further motivated because (in contrast with, e.g., the last interglacial maximum) there is sufficient palaeodata available for 6 kyr BP to permit a detailed reconstruction of regional climates.

The 6 kyr BP experiment is not intended to reproduce all aspects of the climate of 6 kyr BP. Sensitivity experiments have already shown that sea-ice, vegetation, and surface hydrological feedbacks can significantly modify insolation-induced climate changes at both high and low latitudes (Gallimore and Kutzbach 1989; Street-Perrott et al. 1990; Foley et al. 1994; TEMPO 1996; Kutzbach et al. 1996; Texier et al. 1997; Claussen and Gaylor 1997). Comparisons of PMIP 6 kyr BP simulations with palaeoclimatic observations nevertheless can show the extent to which land surface energy balance and associated atmospheric circulation changes can account for the robust features of the palaeoclimate (cf. Jolly et al. 1998a).

One model intercomparison approach adopted by PMIP is to use the output from the climate simulations to drive an equilibrium vegetation model, specifically the BIOME model of Prentice et al. (1992). The BIOME model is an effective diagnostic tool because it provides a method of synthesizing the effects of seasonal changes in both temperature and moisture balance in a single map. Consideration of the direction of the simulated vegetation changes often makes it possible to isolate the seasonal component of the climate anomaly that is most important in a particular region. The BIOME model has been used to compare control runs of successive versions of the ECHAM AGCM (Claussen and Esch 1993) and to analyze the differences between 126 kyr and 115 kyr BP conditions, representing an extreme contrast of orbital parameters, as simulated with a version of the Community Climate Model (CCM1) (Harrison et al. 1995).

In this paper, we present biome distributions derived from 10 PMIP simulations. Analysis of these results allows us to (a) quantify the simulated response to orbital forcing as measured by vegetation change, (b) identify robust features of the PMIP 6 kyr BP experiment, (c) identify regional differences among simulations, and (d) make an initial comparison of the results with palaeoclimatic data for 6 kyr BP. We do not address the question of what causes the differences between model predictions at the regional scale; this is the subject of ongoing analyses in PMIP (Joussaume et al. 1998, unpublished manuscript). A detailed and quantitative assessment of the degree to which the PMIP simulations reproduce observed biome changes is not yet possible—this must await the completion of the global palaeovegetation datasets currently being compiled within the framework of the BIOME 6000 project (Prentice and Webb 1998); however, we have been able to use published comprehensive summaries of regional vegetation changes, including some regional datasets produced by the BIOME 6000 project.

2. The PMIP 6 kyr BP experiment

The 6 kyr BP simulations differ from the control simulations (Table 1) in only two respects: orbital param-

TABLE 1. PMIP 6 kyr BP boundary conditions.

Boundary conditions	Modern (control)	6 kyr BP
Sea surface temperatures	Modern control run *or* 10-yr average (1979–88) of AMIP dataset	As modern
Sea ice	Modern control run *or* 10-yr average (1979–88) of AMIP dataset	As modern
Land albedo	Modern control run	As modern
Ice sheets	Modern control run	As modern
Topography–coastlines	Modern control run	As modern
CO_2	Modern control run *or* 345 ppmv	280/345 × modern control run *or* 280 ppmv
Insolation	Solar constant: modern control run *or* 1365W m^{-2} $e = 0.016724$ $\varepsilon = 23.446°$ Angle between autumn equinox and perihelion = 102.04°	Solar constant: as modern $e = 0.018682$ $\varepsilon = 24.105°$ Angle between autumn equinox and perihelion = 0.87°
Seasonal cycle	Yes	Yes
Number of years simulated	Minimum of 11 yr (average of last 10 yr)	Minimum of 11 yr (average of last 10 yr)

eters were changed, and atmospheric CO_2 concentration was lowered to the preindustrial level. Since the sea surface temperatures (SSTs) are not changed, the lowering of CO_2 is assumed to have only a minor effect (Hewitt and Mitchell 1996). Orbital parameters in the control experiment were specified for 1950 A.D. (eccentricity: 0.016724; obliquity: 23.446°; angle between autumn equinox and perihelion: 102.04°). The orbital parameters at 6 kyr BP were specified following Berger (1978) (eccentricity: 0.018682; obliquity: 24.105°; angle between autumn equinox and perihelion: 0.87°). The vernal equinox was defined as 1200 solar time 21 March, and the longitude of perihelion was defined relative to the vernal equinox—180°. The lengths of the calendar months used for calculating the results were held the same as in the control. The atmospheric CO_2 concentration was specified as 345 ppmv in the control case and 280 ppmv at 6 kyr BP. However, in the case of those groups that made use of an existing control run (UKMO HADAM2, CCM2), the 6 kyr BP CO_2 level is 280/345 of the level in the control. All the simulations were made with sea surface conditions (SSTs and the extent and duration of sea ice) prescribed as for the modern control run. Land surface conditions (the distribution of land and land ice, albedo, and surface roughness) were also prescribed as in the control run.

3. The climate models

The modern control and 6 kyr BP climate simulations used in this study have been run with version 2.0 of the U.K. Universities Global Atmospheric Modelling Programme (UGAMP) model (Hall and Valdes 1997), version 3.2 of the U.K. Meteorological Office (UKMO) model (HADAM2: Hewitt and Mitchell 1996), version 3.2 of the European Center, Hamburg (ECHAM) model (K. Herterich 1995, unpublished manuscript), version 2 of the GENESIS model (GENESIS2; Thompson and Pollard 1997), a version of the University of Tokyo climate model (CCSR1; A. Abe-Ouchi 1995, unpublished manuscript), two versions of the the National Center for Atmospheric Research CCM (a modification of CCM2 and CCM3), and three versions of the Laboratoire de Météorologie Dynamique (LMD) model as run at the Laboratoire de Modélisation du Climat et de l'Environnement (LMD-LMCE 4ter, LMD-LMCE 5.3, and LMD-LMCE 5.3 modified; N. de Noblet and S. Joussaume 1995, unpublished manuscript). The modified version of CCM2 (Hack et al. 1993; Hack et al. 1994; Kiehl 1994) incorporates a land surface model (LSM) with an explicit treatment of vegetation and soil processes (Bonan 1995a,b). The CCM3 (Kiehl et al. 1996) includes several modifications relative to CCM2: improved radiation and cloud parameterizations, and improved treatment of deep convection and the atmospheric boundary layer; it uses the land surface model of Bonan (1996). The two versions of the LMD model differ in their surface schemes and surface flux parameterizations (Table 2): version 4ter uses a simple bucket model for the computation of soil moisture whereas version 5.3 uses the SECHIBA land surface scheme (Ducoudré et al. 1993). The original 5.3 version differentiates eight vegetation types, whereas the modified version (LMD-LMCE 5.3mod) uses the same 17 vegetation types as in the BIOME Model (see below). Version 5.3mod also includes a more realistic treatment of canopy conductance and seasonal variations of leaf area index, and the effects of these variations on land–atmosphere energy and water exchanges (de Noblet et al. 1996).

The UGAMP 2.0, ECHAM 3.2, CCM2, and CCM3 AGCMs are spectral models, using a triangular truncation at wavenumber 42 (T42) and thus corresponding to a latitude–longitude grid of 64 × 128 points (~2.8° × ~2.8°). GENESIS2 has a resolution of T31 (3.75° × 3.75°) and is coupled to a gridpoint land surface model with a resolution of 2° × 2°. CCSR1 has a resolution of T21 (~5.62° × ~5.62°). The UKMO and LMD AGCMs are gridpoint models. The UKMO HADAM2 model has a latitude–longitude grid of 73 × 96 points (~2.5° × ~3.75°). The LMD model employs a grid that is regular in the sine of latitude, such that each grid cell has the same area. LMD-LMCE 4ter has a latitude–longitude grid of 36 × 48 points (~5° lat × ~7.5° long at 50°N), and the two versions of LMD-LMCE 5.3 have

TABLE 2. Summary of the treatment of various aspects of the land surface in the climate models.

	Land surface	Snow cover	Vegetation	Soil hydrology
UKMO HADAM2	Geographically varying soil and vegetation types diagnosed from Wilson and Henderson-Sellers (1985)	Explicit budget	Explicit vegetation, canopy interception model (Warrilow et al. 1986)	Single layer, with spatially nonuniform water-holding capacity (Gregory and Smith 1990)
UGAMP 2.0	Undifferentiated	Explicit budget; snowmelt >0°C T_{snow} surface	Not explicit; albedo from satellite data (Preuss and Geleyn 1980; Geleyn and Preuss 1983)	3-layer diffusive scheme, no-flux lower boundary
ECHAM 3.2	Fractional area of vegetation (not distinguished by type) from Wilson and Henderson-Sellers (1985)	Explicit budget; fractional area is function of depth; snowmelt >0°C T_{ground}	Not explicit; albedo from satellite data (Preuss and Geleyn 1980; Geleyn and Preuss 1983)	3-layer diffusive scheme (Blondin and Böttger 1987)
CCM2	28 different surface types, plus lakes and wetlands	Explicit budget; fractional area is function of depth; snowmelt >+2°C T_{ground}	Explicit vegetation canopy model (Bonan 1995a, 1996)	6-layer diffusive scheme (Bonan 1996)
CCM3	28 different surface types, plus lakes and wetlands	Explicit budget; fractional area is function of depth; snowmelt >0°C T_{ground}	Explicit vegetation canopy model (Bonan 1996)	6-layer diffusive scheme (Bonan 1996)
LMD-LMCE 4ter	Undifferentiated	Explicit budget; snowmelt >0°C T_{ground}	Not explicit; albedo from climatology (Bartman 1980)	Single-layer bucket (Budyko 1956), with uniform 0.15-m water-holding capacity
LMD-LMCE 5.3	Mosaic vegetation (8 different types plus bare ground) prescribed from Matthews (1983); undifferentiated soil	Explicit budget; fractional area is function of depth; snowmelt >0°C T_{ground}	Explicit vegetation; canopy model (Ducoudré et al. 1993)	2-layer nondiffusive scheme (Choisnel 1984)
LMD-LMCE 5.3mod	Mosaic vegetation (17 different biomes plus bare ground) from simulation of BIOME1 forced with climatology of Leemans and Cramer (1991); undifferentiated soil	Explicit budget; fractional area is function of depth; snowmelt >0°C T_{ground}	Explicit vegetation; canopy model (Ducoudré et al. 1993), modified (de Noblet et al. 1996)	2-layer nondiffusive scheme (Choisnel 1984)
GENESIS2	Mosaic vegetation (110 plant forms plus bare ground) from simulations of vegetation model forced with modern climatology (Bergengren and Thompson 1996, personal communication	Explicit budget; fractional area is function of depth; snowmelt >0°C, snow temperature within 3-layer snow model	Explicit vegetation, canopy model (Pollard and Thompson 1995)	6-layer diffusive scheme (Pollard and Thompson 1995)
CCSR1	Undifferentiated	Explicit budget; snowmelt >0°C T_{snow} surface	Not explicit; albedo for different vegetation types after Matthews (1983)	Single-layer bucket (Manabe et al. 1965), with uniform 0.15-m water-holding capacity

TABLE 3. Characteristics of the control and 6 kyr BP model simulations.

Model	Simulation	Resolution	CO^2 (ppmv)	SSTs	Length of run (yr)	Ensemble average (yr)
UKMO HADAM2	Control	73 × 96	323	UKMO dataset	31	30
UKMO HADAM2	6000 yr BP	73 × 96	262	UKMO dataset	31	30
UGAMP 2.0	Control	64 × 128	345	Alexander and Mobley (1976)	11	10
UGAMP 2.0	6000 yr BP	64 × 128	280	Alexander and Mobley (1976)	11	10
ECHAM 3.2	Control	64 × 128	345	PMIP standard	30	10
ECHAM 3.2	6000 yr BP	64 × 128	280	PMIP standard	15	10
CCM2	Control	64 × 128	355	PMIP standard	10	10
CCM2	6000 yr BP	64 × 128	288	PMIP standard	10	10
CCM3	Control	64 × 128	355	Shea et al. (1990)	8	8
CCM3	6000 yr BP	64 × 128	288	Shea et al. (1990)	8	8
LMD-LMCE 4ter	Control	36 × 48	345	PMIP standard	16	15
LMD-LMCE 4ter	6000 yr BP	36 × 48	280	PMIP standard	16	15
LMD-LMCE5.3	Control	50 × 64	345	PMIP standard	16	15
LMD-LMCE5.3	6000 yr BP	50 × 64	280	PMIP standard	16	15
LMD-LMCE5.3mod	Control	50 × 64	345	PMIP standard	16	15
LMD-LMCE5.3mod	6000 yr BP	50 × 64	280	PMIP standard	16	15
GENESIS2	Control	48 × 96*	345	Shea et al. (1990)	10	10
GENESIS2	6000 yr BP	48 × 96*	280	Shea et al. (1990)	10	10
CCSR1	Control	32 × 64	345	PMIP standard	15	10
CCSR1	6000 yr BP	32 × 64	280	PMIP standard	15	10

* Surface process model (LSX) is 2° × 2° or 90 × 180 grid points.

a grid of 50 × 64 points (~3.5° lat × 5.265° long at 50°N).

With one exception, each climate model was run for a minimum of 10 yr and the derived climate variables are the ensemble average of a minimum of 10 yr (Table 3).

4. Application of the BIOME model

The AGCM simulations have been translated into simulated natural vegetation using the biome model (BIOME) of Prentice et al. (1992). BIOME is a model developed from physiological considerations to predict global patterns in potential vegetation physiognomy as a function of climate (Prentice et al. 1992). In the model, the main constraints on the growth and regeneration of different plant functional types are formulated in terms of limiting values of the mean temperature of the coldest and warmest months, ''growing'' degree-days, and a coefficient (the Priestley–Taylor coefficient: α) for the extent to which soil moisture supply satisfies atmospheric moisture demand. These bioclimatic indices are calculated from an input climate dataset of mean monthly temperature, precipitation, and sunshine fraction. Biomes emerge from the combination of different plant functional types.

Two procedures are currently used to derive input climate fields for the BIOME model. In the first (e.g., Prentice et al. 1994; Harrison et al. 1995; TEMPO 1996; de Noblet et al. 1996; Kutzbach et al. 1996; Kutzbach et al. 1997; Texier et al. 1997), AGCM anomalies (the difference between a perturbed climate and the modern control simulation) are interpolated to the grid commonly used in the BIOME model (0.5°) and then superimposed on a modern climate dataset. This procedure was originally designed with the idea that the use of AGCM anomalies would reduce the effects of systematic model biases, whereas adding the anomalies to a modern dataset (which incorporates the effects of topography on climate) would make it possible to capture some of the local-scale spatial pattern due to terrestrial geography (e.g., the effects of a given climate anomaly on vegetation at different elevations). In the second procedure (e.g., Claussen and Esch 1993; Claussen 1996; Claussen 1997; Claussen and Gaylor 1997), the BIOME model is run directly from the simulated climate on the AGCM's own grid.

We have run a set of eight simulations, using output from the ECHAM 3.2 model, to test whether the choice of procedure is likely to affect our estimates of the magnitude of the simulated vegetation changes at 6 kyr BP. In the first set of experiments, the BIOME model was run directly using climate data from the control (Fig. 1a) and the 6 kyr BP (Fig. 1b) simulations. In the second set of experiments, climate data from the control (Fig. 1c) and 6 kyr BP (Fig. 1d) simulations were interpolated to the 0.5° grid of the BIOME model and then used to run the BIOME model. In the third set of experiments (Figs. 1e and 1f), AGCM anomalies were superimposed on a modern climate dataset [an extended version of Leemans and Cramer (1991) and based on ca. 9000 meteorological stations], which had been interpolated to the AGCM grid. In the final set of experiments (Figs. 1g and 1h), the AGCM anomalies were first interpolated to the BIOME model grid and then superimposed on the Leemans and Cramer (1991) dataset. This set of simulations enables us to examine separately the use of interpolation and the use of an anomaly procedure.

FIG. 1. Biome maps simulated using different procedures to derive input fields for the BIOME maps: (a) the BIOME model was run at the AGCM grid scale using climate data directly from the ECHAM 3.2 control simulation; (b) the BIOME model was run at the AGCM grid scale using climate data from the ECHAM 3.2 6 kyr BP simulation; (c) the BIOME model was run on a 0.5° grid, using climate data from the ECHAM 3.2 control simulation, which had been interpolated to the 0.5° grid; (d) the BIOME model was run on a 0.5° grid, using climate data from the ECHAM 3.2 6 kyr BP simulation, which had been interpolated to the 0.5° grid; (e) the BIOME model was run using the modern climate dataset interpolated to the AGCM grid; (f) the BIOME model was run at the AGCM grid scale, using a climate dataset created by adding the anomalies between the ECHAM 3.2 control and 6 kyr BP experiment to the modern climate dataset shown in panel e; (g) the BIOME model was run using the modern climate dataset interpolated to the 0.5° grid; (h) the BIOME model was run at the 0.5° grid, using a climate dataset created by adding the anomalies between the ECHAM 3.2 control and 6 kyr BP experiment to the modern climate dataset shown in panel g.

FIG. 1. (*Continued*)

TABLE 4. Quantitative changes in vegetation patterns at 6 kyr BP simulated using different procedures for deriving climate data from the ECHAM 3.2 model to run the BIOME model, as measured by the kappa statistic. The columns indicate whether the climate data were applied at the scale of the AGCM grid (AGCM grid) or at the scale of the BIOME model grid (0.5° grid), the rows indicate whether the BIOME simulations were run with climate data from the control and 6 kyr BP experiments (direct) or using the anomalies between the control and 6 kyr BP experiments superimposed on a modern climate dataset (anomaly).

	Global		N. extratropics		Intertropical zone		S. extratropics	
	AGCM grid	0.5° grid	AGCM grid	0.5° grid	AGCM grid	0.5° grid	AGCM grid	0.5° grid
Direct	0.78	0.77	0.74	0.73	0.79	0.79	0.81	0.80
Anomaly	0.75	0.75	0.72	0.72	0.74	0.76	0.77	0.83

To assess whether the different procedures yield quantitatively different magnitudes of vegetation change, we have compared the global biome maps using the kappa statistic to assess agreement (Cohen 1960; Monserud 1990; Prentice et al. 1992). The kappa statistic provides a measure of the agreement between two maps, based on the proportion of the total number of grid cells assigned to the same category (in this case, the same biome) and after taking account of the number of grid cells that might be expected to be the same due to chance alone. It is possible to assess the statistical significance of the kappa value; however, in cases where there are a very large number of grid cells such that almost any two maps will be different at a high level of significance, such tests are not very useful. Monserud (1990) proposed a subjective assessment scale, in which kappa values of <0.4 are considered to indicate a very poor match between two maps: 0.4–0.55 a fair match, 0.55–0.7 a good match, 0.7–0.85 a very good match, and >0.85 an excellent match. This subjective scheme has been used for other assessments of simulated biome maps (e.g., Prentice et al. 1992; Monserud and Leemans 1992) and is used here.

Clearly, there are differences between the biome maps produced by the various procedures. Using the AGCM climate directly results in, for example, the Sahara–Sahel boundary being placed further north at 6 kyr BP (Figs. 1b and 1d) than in the simulations using the anomaly procedure (Figs. 1f and 1h), while at the same time showing the tundra/forest boundary in North America and northern Eurasia substantially further south than in the anomaly procedure simulation. However, examination of the biome maps produced directly from the control simulations (Figs. 1a and 1c) shows that these regions are characterized by systematic model biases: the southern Sahara is too wet in the control simulation and the northern high latitudes are too cold, such that the simulated biomes are systematically different from the modern observed vegetation.

The interpolation procedure, while it seems to have some local effects (e.g., in mountainous areas) on the vegetation distribution, produces a negligible difference in the kappa estimates of the magnitude of change between the modern (or control) situation and 6 kyr BP (Table 4). The kappa values differ by 0.01 in the case where the BIOME model was run directly from AGCM output and 0.02 in the case where the anomaly procedure is used. The only exception is for regions (e.g., the southern extratropics) where the total land area (and hence the number of grid cells being compared) is rather small. Even in this case, the maximum difference between the kappa values is only 0.06. The difference in the kappa values obtained when comparing the BIOME simulations obtained directly from the control and 6 kyr BP simulations and those made using the anomaly procedure is <0.05, whether the comparison is made at the scale of the AGCM grid or at the 0.5° grid of the BIOME model. The kappa values using the anomaly procedure are almost always smaller (i.e., imply a larger change between the 6 kyr BP and modern/control situations) than those obtained directly using AGCM output, implying that the anomaly procedure is less conservative than running the BIOME model directly from AGCM output. Thus, these analyses show that the choice of procedure does not significantly affect the estimates of the magnitude of vegetation change. However, using the anomaly procedure clearly reduces the effect of systematic climate model bias on the resulting biome maps. While this may not be an advantage in making model–model comparisons, it is necessary if the biome simulations are to be used for comparisons with palaeoenvironmental data.

Thus, in our analyses of the PMIP 6 kyr BP simulations we have adopted the procedure of using AGCM anomalies of mean monthly temperature, precipitation, and cloudiness, interpolated to the 0.5° grid of the BIOME model, and superimposed on a modern climate dataset specified from an extended version of Leemans and Cramer (1991) in order to maximize the usefulness of the resulting simulated biome maps for comparisons with reconstructions of past vegetation patterns. We have compared the global biome maps with the vegetation patterns simulated by BIOME from climatological data using the simple kappa statistic to assess agreement (Prentice et al. 1992).

5. Results

a. Description of simulated BIOME maps

The biome maps generated from the 10 AGCM simulations for 6 kyr BP are shown in Fig. 2. When compared with the modern simulated vegetation (Fig. 1g), the most significant features of the 6 kyr BP simulations

FIG. 2. Simulated 6 kyr BP biomes.

FIG. 2. (*Continued*)

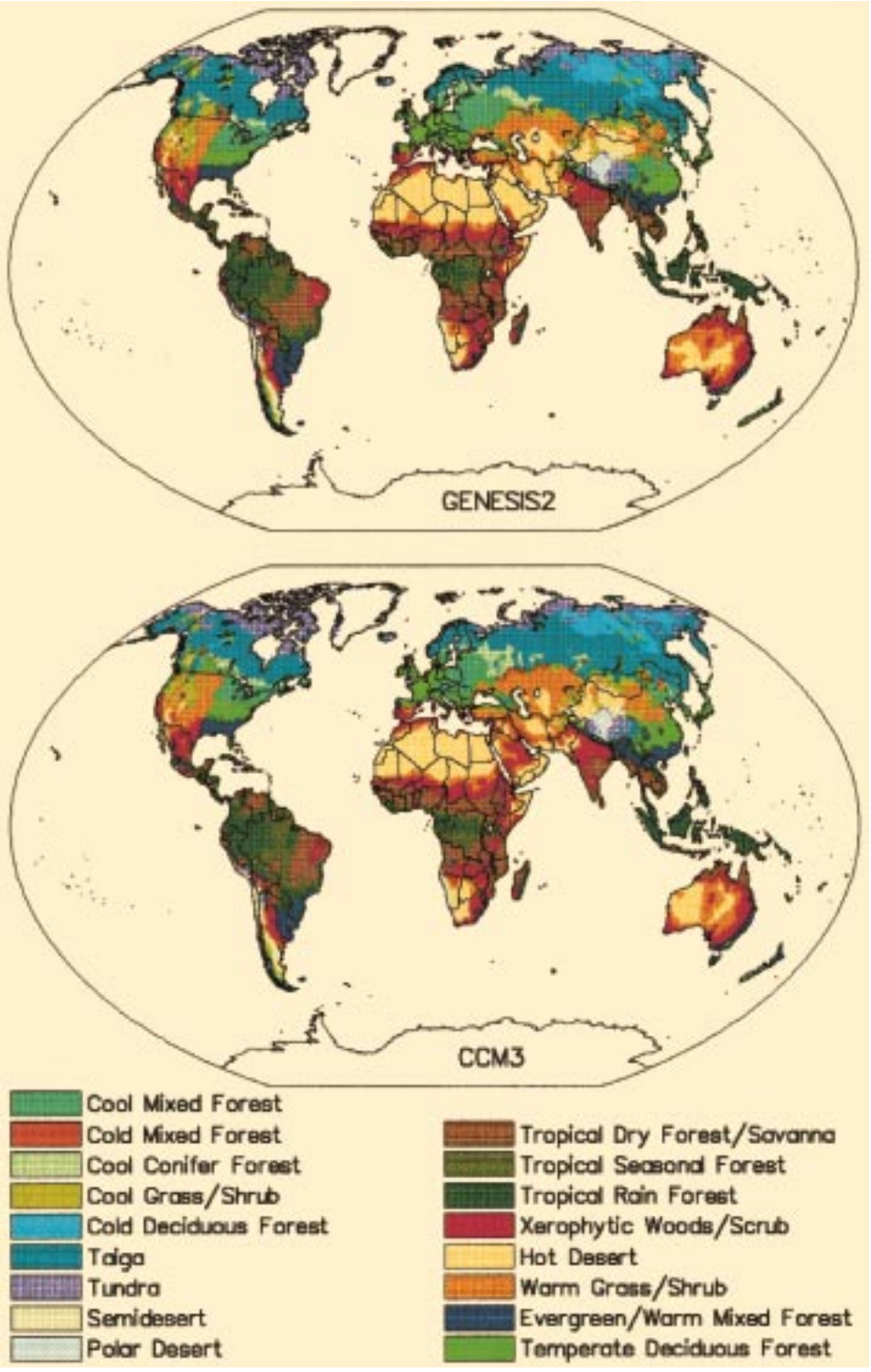

FIG. 2. (*Continued*)

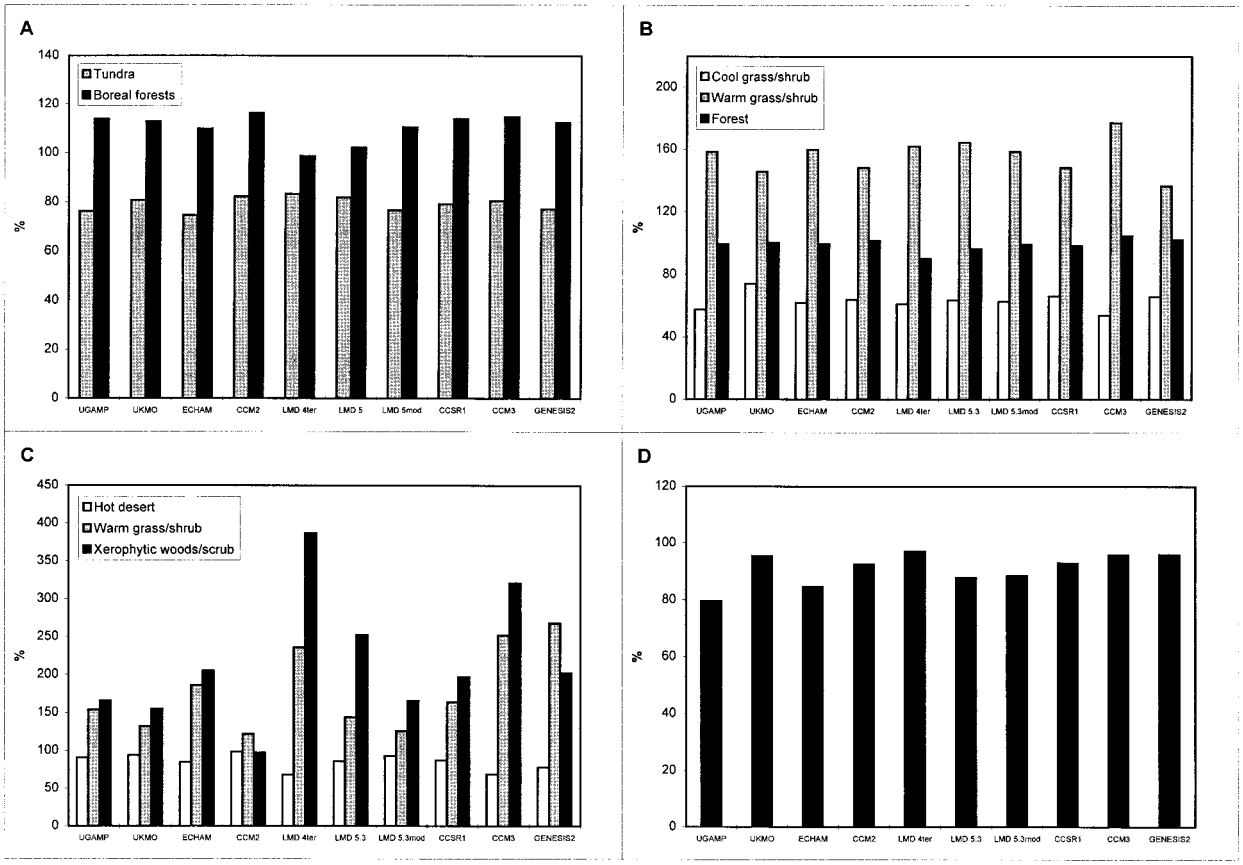

FIG. 3. Change in area of key biomes at 6 kyr BP, as expressed as a percentage of their modern extent. (a) Changes in the area of tundra and boreal forests in the region north of 30°N. Boreal forests are defined to include the taiga and cold deciduous forest biomes. (b) Changes in the area of warm grass/shrub, cool grass/shrub, and forest in the zone between 30° and 55°N. Forest is defined to include taiga, cold deciduous forest, cool conifer forest, cold mixed forest, cool mixed forest, temperate deciduous forest, and evergreen warm/mixed forest. (c) Changes in the area of desert, warm grass/shrub, and xerophytic woods/scrub in the African Sahelian zone (14°–22°N). (d) Changes in the area of tropical rain forest.

are vegetation changes reflecting high-latitude warming in the Northern Hemisphere, Northern Hemisphere midlatitude winter cooling, Northern Hemisphere midcontinental warming/aridity, the expansion of the Afro–Asian monsoon, and equatorial aridity.

1) HIGH-LATITUDE SUMMER WARMING

All of the simulations show a general northward displacement of the high-latitude forest belts. Tundra is reduced to 74%–83% of its modern area (Fig. 3a). Cool conifer forests encroach northward, displacing taiga along its present southern margin, for example, in Fennoscandia. Cool mixed forests also occur farther north than today, particularly in Fennoscandia and European Russia. The simulated northward shifts in the high-latitude forest belts reflect a general increase in the warmth of the growing season. The most extreme shifts overall in the vegetation zones (reflecting the largest high-latitude warming), are shown by the ECHAM 3.2 simulation, where the tundra is reduced to 74% of its modern extent while boreal forests (taiga and cold deciduous forest) expand to 113% of their modern extent. Although some of the simulations show a northward shift of the southern boundary of taiga in eastern North America in response to summer warming, in others this effect is masked by the simulation of cold winters, which prevents this northward shift or even forces a slight southward expansion of taiga.

2) MID- AND HIGH-LATITUDE WINTER COOLING

The UGAMP 2.0, LMD-LMCE 4ter, LMD-LMCE 5.3, and CCSR1 simulations produce a zone of cold deciduous forest in northern Canada, in an area occupied by taiga today, in response to low winter temperatures that exceed the tolerance of evergreen conifers. The simulations also show a southward expansion of taiga and cool conifer forests in Siberia, displacing cool mixed forest, in response to colder winters in the Eurasian continental interior. The expansion is most marked in the LMD-LMCE 4ter simulation. Midlatitude winter

cooling is registered in all the simulations by a southward expansion of temperate deciduous forests, at the expense of evergreen/warm mixed forests, in China. Most of the simulations show a southward expansion of cool mixed forest, displacing temperate deciduous forest, in eastern North America in response to winter cooling. In some cases (e.g., UGAMP 2.0) this cooling is sufficient to allow temperate deciduous forests to expand southward into the zone occupied today by evergreen/warm mixed forests.

3) MIDCONTINENTAL WARMING/ARIDITY

Northern Hemisphere midcontinental summer warming is expressed in all the models as an expansion of warm grass/shrub at the expense of cool grass/shrub (Fig. 3b). Aridity, associated with this warming, is expressed by the expansion of grass/shrub at the expense of forest biomes. In the zone between 30° and 55°N, warm grass/shrub expands to between 137% (GENESIS2) and 177% (CCM3) of its modern extent, while cool grass/shrub decreases to between 74% (UKMO HADAM2) and 54% (CCM3).

In North America, simulated midcontinental warming is shown by the northward and westward extension of warm grass/shrub, rather than by a shift in the prairie–forest boundary in the Midwest. The change is most pronounced in the ECHAM 3.2 and CCM2 simulations. In central Eurasia, the extension of warm grass/shrub at the expense of cool grass/shrub is most pronounced in the UGAMP 2.0, LMD-LMCE 4ter, and CCSR1 models. The midcontinental warming appears to be associated with changes in regional water budgets, expressed in changes in the distribution of forest and nonforest biomes. The location of zones of increased/decreased effective moisture varies from model to model, but most of the simulations show a northwestward retreat of the forest limit in eastern Europe, to the north of the Black Sea, and a northeastward retreat of taiga in central Siberia.

4) THE AFRO–ASIAN MONSOON

The expansion of the Afro–Asia monsoon is expressed by the expansion of moisture-demanding biomes at the expense of more drought-tolerant biomes. This shift involves different biomes in different regions. Changes in the extent of deserts provides one simple measure of the magnitude of monsoon expansion. According to these simulations, the area of Northern Hemisphere deserts was reduced to between 77% (CCM3) and 99% (UGAMP 2.0) of its modern extent.

Monsoon expansion in Africa is indicated in all the models as a northward shift in xerophytic woods/scrub and warm grass/shrub, at the southern margin of the Sahara. The northward displacement is largest in the ECHAM 3.2, CCM3, GENESIS2, and LMD-LMCE 4ter simulations. In the Sahelian zone (14°–22°N), the desert is reduced to 68% of its present extent in the LMD-LMCE 4ter simulation, to 69% in the CCM3, to 78% in the GENESIS2, and to 81% in the ECHAM 3.2 simulation (Fig. 3c). The smallest reduction in the area of desert in this zone is shown by CCM2 (98% of modern). The northward shift is generally accompanied by drying on the southern margin of the Sahel, shown by the expansion of xerophytic woods/scrub southward at the expense of tropical closed forests. This is because the monsoon expansion is related to a northward shift of the ITCZ in summer. There is no indication of drying on the southern margin of the Sahel in the UKMO HADAM2 simulation, however, because the simulated changes in the moisture budget are small and insufficient to produce a shift from tropical dry forest to xerophytic woods/scrub.

The simulated vegetation changes in response to the expansion of the Asian monsoon are less coherent between the models than the changes in northern Africa. In the ECHAM 3.2 and CCM2 simulations, there is a noticeable expansion of tropical dry forest/savanna (at the expense of xerophytic woods/scrub) in southern India. Several of the models (ECHAM 3.2, CCM3, LMD-LMCE 4ter, LMD-LMCE 5.3, LMD-LMCE 5.3mod, GENESIS2, CCSR1) show an expansion of warm grass/shrub vegetation into areas occupied today by desert in eastern central Asia.

5) EQUATORIAL ARIDITY

The simulated shift in the position of the ITCZ results in increased aridity in the equatorial zone. This is reflected by a reduction in the extent of tropical rain forest (Fig. 3d). The reduction is most marked in the UGAMP 2.0 simulation, where the tropical rain forest is reduced to 79% of its present area, and least marked in the UKMO HADAM2 (95.5%), CCM3 (95.9%), GENESIS2 (96%), and LMD-LMCE 4ter simulations (97%).

The increase in aridity is not uniform within the equatorial zone, and the areas affected vary between the models. All of the models produce a reduction in the area of rain forest in Africa, with the most extreme changes being registered by ECHAM 3.2 and CCM2. Not all of the models produce a significant reduction of the rain forest in South America, but the UGAMP 2.0, ECHAM 3.2, and CCSR1 simulations are characterized by the expansion of tropical dry forest/savanna particularly on the northern and eastern margins of the rain forest. The UKMO HADAM2, ECHAM 3.2, CCM2, CCM3, GENESIS2, and CCSR1 simulations show no change in Oceania, whereas the UGAMP 2.0, LMD-LMCE 4ter, and both versions of LMD-LMCE 5.3 show an increase in tropical seasonal and tropical dry forests at the expense of tropical rain forest in this region. The magnitude of the reduction of tropical rain forest in particular regions is not related to the magnitude of the zonal change in aridity.

TABLE 5. Quantitative change in vegetation patterns at 6 kyr BP compared to the patterns simulated by BIOME from climatological data, as measured by the kappa statistic.

Model	Global	N. extra-tropics	Inter-tropical zone	S. extra-tropics
UKMO HADAM2	0.83	0.80	0.84	0.92
UGAMP 2.0	0.75	0.71	0.78	0.84
ECHAM 3.2	0.75	0.72	0.76	0.83
CCM2	0.79	0.77	0.78	0.87
CCM3	0.75	0.73	0.72	0.85
LMD-LMCE 4ter	0.72	0.68	0.76	0.80
LMD-LMCE5.3	0.76	0.72	0.77	0.85
LMD-LMCE5.3mod	0.80	0.77	0.80	0.89
GENESIS2	0.80	0.78	0.79	0.86
CCSR1	0.82	0.78	0.84	0.88

6) THE SOUTHERN HEMISPHERE EXTRATROPICS

According to these simulations, vegetation changes in the southern extratropical zone of South America and Africa are extremely small. This presumably reflects the use of prescribed (modern) ocean conditions and the relatively small areas of the Southern Hemisphere continents that are influenced by insolation changes. However, the situation is different for Australia. Although some of the simulations (UKMO HADAM2, CCM2, CCSR1) show virtually no change from present, changes in the extent of the desert in the other simulations indicate both increasing (UGAMP 2.0, ECHAM 3.2, LMD-LMCE 5.3mod) and decreasing aridity (CCM3, LMD-LMCE 4ter, LMD-LMCE 5.3, GENESIS2).

b. Kappa statistics

At a global scale, the changes in simulated biome distributions are small (Table 5). The simulations yield kappa values in the range of 0.72–0.83. According to the subjective scale proposed by Monserud (1990), these values indicate a very good match to the modern biome map. The UKMO HADAM2 simulation, with a kappa value of 0.83, shows the smallest changes compared to present, whereas the LMD-LMCE 4ter model (0.72) shows the largest changes. Comparison of the simulated vegetation changes within the Tropics yield kappa values between 0.72 (CCM3) and 0.84 (UKMO HADAM2), indicative of a very good match to the modern vegetation map. The range for the northern extratropics is between 0.68 (LMD-LMCE 4ter) and 0.80 (UKMO HADAM2) and indicates a good to very good match, whereas the range for the southern extratropics is between 0.80 (LMD-LMCE 4ter) and 0.92 (UKMO HADAM2) and thus shows a very good to excellent match with the modern vegetation map.

We tested whether the apparent differences between the models could be related to the difference in the length of the runs, and hence the number of years used to derive an ensemble average climate to drive the BIOME model (Table 3), using output from the 30-yr simulation made with the UKMO HADAM2 model. We ran three BIOME simulations, driven by the ensemble averages independently derived from the first, second, and third decades of the UKMO HADAM2 simulation. The difference in the kappa values was small at the global scale (0.80, 0.82, 0.83, respectively), for the northern extratropics (0.76, 0.79, 0.80), intertropical zone (0.81, 0.83, 0.83) and the southern extratropics (0.86, 0.91, 0.91), and smaller than the difference between the 6 kyr BP simulation and modern conditions. This confirms that the simulated biomes are stable, and shows that the comparatively small changes shown by the UKMO HADAM2 model are not related to the fact that the simulation was run for a longer time than the others.

We have also used the kappa statistic to compare the 6 kyr BP simulations in order to assess whether the differences between the models are significant. Pairwise comparisons of each of the 6 kyr BP simulations (Table 6) show kappa values ranging from 0.72 to 0.85 at the global scale, from 0.69 to 0.84 for the northern extratropics, from 0.68 to 0.85 in the intertropical zone, and from 0.74 to 0.88 in the southern extratropics. Again, these values show a good to excellent agreement between the models at global and zonal scales. Not unexpectedly, those models that show the biggest changes (e.g., LMD-LMCE 4ter, CCM3) are consistently the most different from the other simulations, and those that

TABLE 6. Pairwise intercomparisons between the 10 models of the quantitative differences in vegetation patterns at 6 kyr BP, as measured by the kappa statistic.

	UKMO HADAM2	UGAMP 2.0	ECHAM 3.2	CCM2	CCM3	LMD-LMCE 4ter	LMD-LMCE 5.3	LMD-LMCE 5.3mod	GENESIS2	CCSR1
UKMO HADAM2	1	0,80	0,80	0,83	0,78	0,75	0,82	0,81	0,84	0,85
UGAMP 2.0	0,80	1	0,77	0,77	0,73	0,72	0,79	0,79	0,80	0,78
ECHAM 3.2	0,80	0,77	1	0,74	0,75	0,72	0,77	0,76	0,79	0,78
CCM2	0,83	0,77	0,74	1	0,75	0,73	0,79	0,77	0,80	0,81
CCM3	0,78	0,73	0,75	0,75	1	0,70	0,75	0,73	0,76	0,77
LMD-LMCE 4ter	0,75	0,72	0,72	0,73	0,70	1	0,75	0,73	0,74	0,75
LMD-LMCE5.3	0,82	0,79	0,77	0,79	0,75	0,75	1	0,83	0,81	0,81
LMD-LMCE5.3mod	0,81	0,79	0,76	0,77	0,73	0,73	0,83	1	0,79	0,79
GENESIS2	0,84	0,80	0,79	0,80	0,76	0,74	0,81	0,79	1	0,84
CCSR1	0,85	0,78	0,78	0,81	0,77	0,75	0,81	0,79	0,84	1

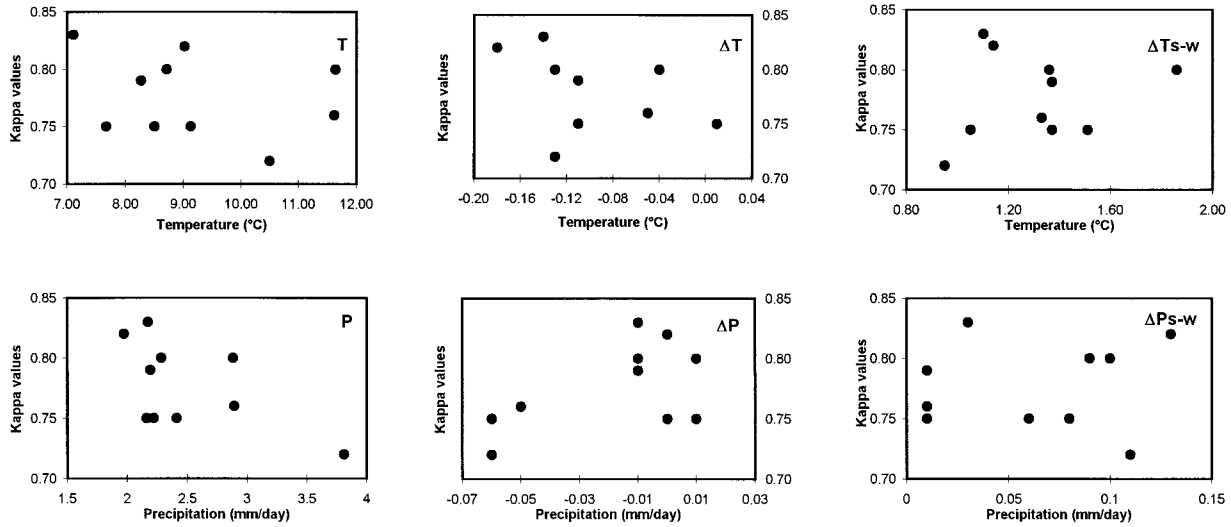

FIG. 4. Comparison of global kappa values and global land surface climate variables: where T is annual average land temperature at 6 kyr BP, ΔT is the land temperature anomaly between 6 kyr and the control simulation, $\Delta T_{s\text{-}w}$ is the change in the seasonal range (the mean temperature for June–August minus the mean temperature for December–February) of land temperature; P is the annual average land precipitation, ΔP is the land precipitation anomaly between 6 kyr BP and the control simulation, $\Delta P_{s\text{-}w}$ is the change in the seasonal range (the mean precipitation for June–August minus the mean precipitation for December–February) of land precipitation.

show the smallest changes (e.g., UKMO HADAM2) are consistently the most similar to other models. Since the possibilities for divergence between the models become greater as the simulated vegetation patterns become more different from the observed modern vegetation pattern, diagnostic analyses of the causes of intermodel differences are likely to be more informative when made at the regional scale and for regions where the changes from present are large.

The simulated changes in vegetation distribution are a response to seasonal changes in, particularly, temperature and precipitation. However, when global or zonal averages of the key climatic variables (e.g., mean annual temperature, mean annual precipitation, the range of seasonal temperature or seasonal precipitation, or the changes in these measures relative to today) are compared to the kappa values, there is no discernible trend between the simulations (Fig. 4, Fig. 5). Thus, it is not

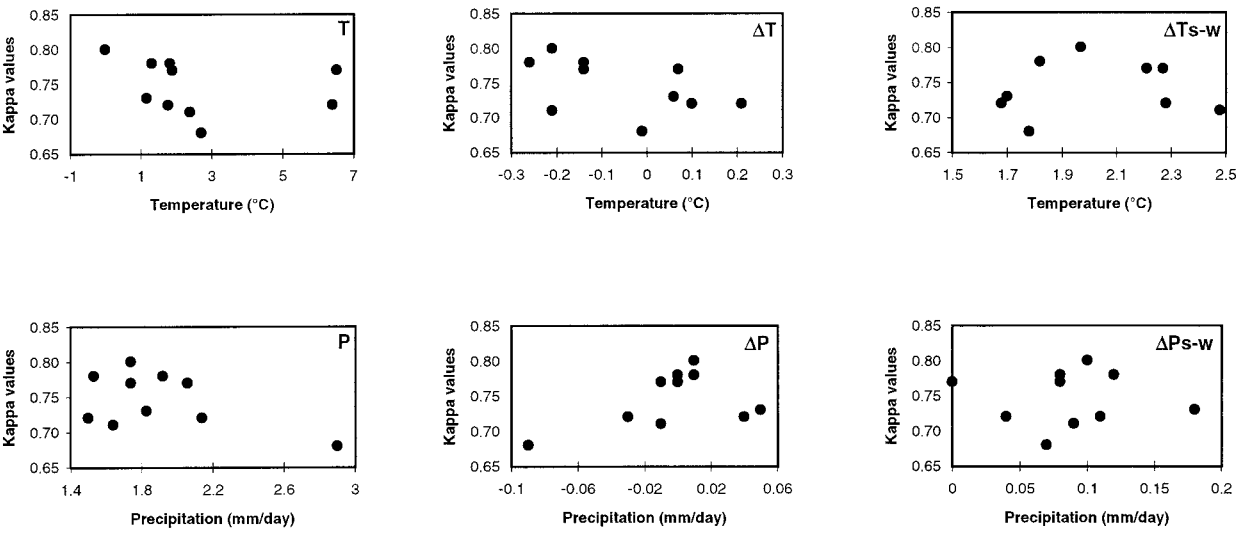

FIG. 5. Comparison of kappa values and land surface climate variables for the Northern Hemisphere extratropics: where T is annual average land temperature at 6 kyr BP, ΔT is the land temperature anomaly between 6 kyr BP and the control simulation, $\Delta T_{s\text{-}w}$ is the change in the seasonal range (the mean temperature for June–August minus the mean temperature for December–February) of land temperature; P is the annual average land precipitation, and ΔP is the land precipitation anomaly between 6 kyr BP and the control simulation, $\Delta P_{s\text{-}w}$ is the change in the seasonal range (the mean precipitation for June–August minus the mean precipitation for December–February) of land precipitation.

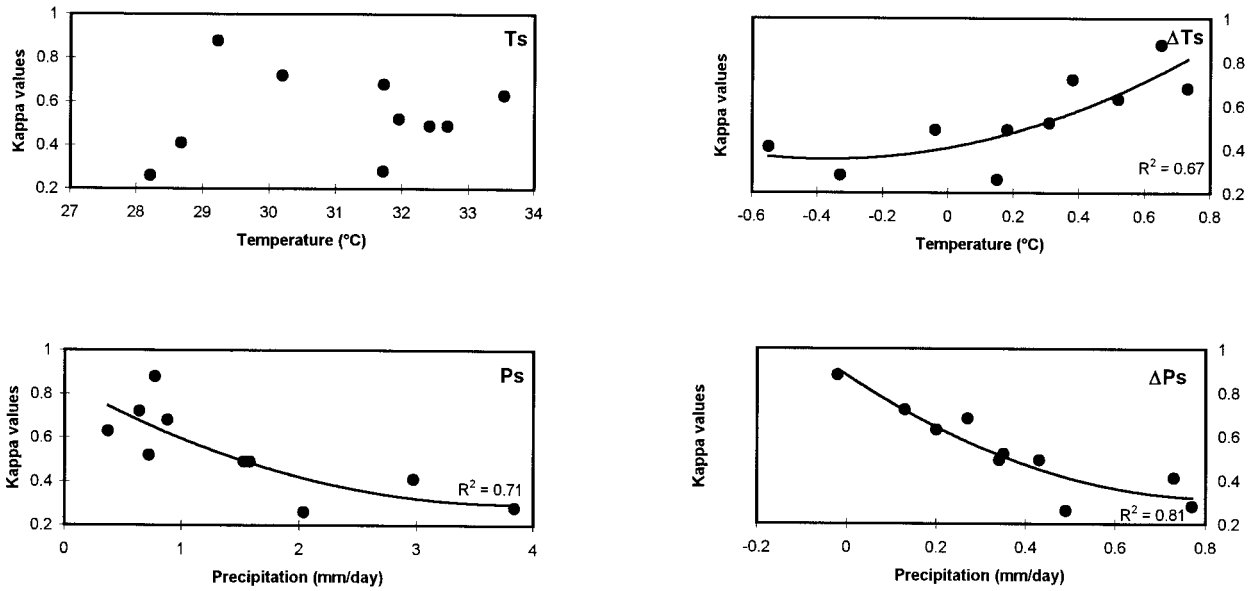

FIG. 6. Comparison of kappa values and land surface climate variables for the African Sahelian zone (14°–22°N), where *Ts* is the mean land temperature for May–October at 6 kyr BP, Δ*Ts* is the land temperature anomaly between the 6 kyr and the control simulation for the same six months, *Ps* is the mean land precipitation for May–October at 6 kyr BP, and Δ*Ps* is the land precipitation anomaly between the 6 kyr and the control simulation for the same 6 months.

possible to demonstrate the relationship between the magnitude of vegetation changes and changes in the driving climate variables at a global or zonal scale. This is partly related to the small differences between the models at global and zonal scales, and partly caused by the difficulty in selecting a region that is characterized by unidirectional climate changes: subcontinental, zonal, and global averages generally mask a high degree of regional variability associated with simulated circulation shifts, which is clearly captured in the biome maps. For example, when climatic variables are compared with kappa values for the Sahelian zone (14°–22°N), there is a clear correlation ($r = 0.81$) between the change in summer (May–October) rainfall and the magnitude of the change in vegetation distribution (Fig. 6). Since the vegetation zonation in this region is strongly controlled by the gradient in α, the relatively strong relationship between the kappa values and the change in summer temperature ($r = 0.67$) reflects the fact that changes in summer temperatures are strongly correlated with changes in precipitation (and hence cloudiness) in this zone. Thus, these analyses demonstrate that it will be necessary to examine relatively small regions, where there are large and significant differences between the simulated vegetation patterns, in order to isolate the specific mechanisms responsible for differences between the simulations.

6. Comparison of the simulated biome changes with palaeoenvironmental observations

The lack of a complete global palaeovegetation dataset for 6 kyr BP at this time prohibits a detailed and quantitative evaluation of the simulated biome changes. Nevertheless, it is possible to examine how far the robust features of the PMIP simulations are qualitatively consistent with observed changes in vegetation distribution as summarized in recent data-synthesis papers.

a. High-latitude summer warming

All of the simulations show a general northward displacement of the high-latitude forest belts, and a concomitant reduction of the area of tundra, as a consequence of an increase in the warmth of the growing season. Pollen and macrofossil data show that the northern limit between forest and tundra at 6 kyr BP was much farther north than today (e.g., Ritchie 1987; Prentice et al. 1996; TEMPO 1996; Tarasov et al. 1998; Texier et al. 1997), except in Alaska (Anderson and Brubaker 1994), parts of northeastern Canada (Richard 1995), and far eastern Siberia (Lohzkin 1993). The largest shifts in the position of the forest–tundra boundary (>300 km) are recorded from the Yamal and Taymyr peninsulas of central Siberia (Tarasov et al. 1998; Texier et al. 1997). All of the models underestimate the northward extension of forests in this region by 4°–5° lat. Pollen-based maps of biome distributions across Europe (Prentice et al. 1996) and northern Eurasia (Tarasov et al. 1998) at 6 kyr BP show two other features indicative of warmer conditions during the growing season: a northward shift in the northern forest belts (e.g., cool conifer forests replacing taiga on the southern margin) and the expansion of cold mixed forests in central Fennoscandia. Although the northward expansion of forest belts is a feature of the PMIP simulations, none of the

models produce an expansion of cold deciduous forests in Fennoscandia. Thus, comparisons with the available palaeovegetation data indicate that the simulated summer warming in the high latitudes is substantially smaller than actually occurred.

b. Mid- and high-latitude winter cooling

The simulations show winter cooling in the midlatitudes, leading to a southward displacement of the forest belts compared to today in, for example, eastern North America, Siberia, and China. At least some of the simulations show an expansion of cold deciduous forest into areas occupied by taiga today in northern Canada, in response to winter cooling at high latitudes. There is insufficient evidence to evaluate whether the simulated expansion of cold deciduous forests in areas currently characterized by taiga in northern Canada is realistic. Pollen data from eastern North America, which show that species characteristic of cool mixed and temperate deciduous forest (e.g., *Picea, Betula, Quercus, Tsuga, Fagus, Ulmus,* and *Carya*) were abundant south of their modern limits (Overpeck et al. 1992; Webb et al. 1993), are consistent with the simulation of winter cooling in the midlatitudes. However, pollen-based biome reconstructions from Siberia show very little change in the southern margin of cool conifer forest, while the southern margin of taiga was slightly farther north than today (Tarasov et al. 1998). Furthermore, pollen-based biome reconstructions from China show that broad-leaved evergreen forest extended ~300 km and temperate deciduous forests ~500–~600 km beyond their present northern limits, implying that the winters were substantially *warmer* than present (Yu et al. 1998). The PMIP simulations do record winter warming in, for example, western Europe, resulting in the simulated position of the northern limit of temperate deciduous forests being up to 200 km north of the observed modern limit. Pollen-based biome reconstructions from Scandinavia indicate that temperate deciduous forests extended >700 km north of their modern limit (Prentice et al. 1996). Thus, even in regions where the PMIP simulations show a significant winter warming, this warming appears to have been substantially less than recorded by the pollen data.

c. Midcontinental warming/aridity

The simulations show conditions both warmer and more arid than today in the midcontinental interior of both North America and Eurasia. The summer warming is registered by an expansion of warm grass/shrub at the expense of cool grass/shrub and the increased aridity by the expansion of grass/shrub at the expense of forest biomes. There are very few pollen data from the midcontinental interior of North America, and this region is not covered by existing palaeoenvironmental syntheses. However, pollen data from adjacent regions of North America (e.g., Webb et al. 1993; Thompson et al. 1993; Ritchie and Harrison 1993) provides evidence of warmer and/or drier conditions, and thus makes the simulated changes in biome distributions appear plausible. For example, pollen-based climate reconstructions using the response-surface method (Bartlein et al. 1986) show an increase in July temperatures of up to 2°C over most of eastern North America (excepting regions near the coast or around the Great Lakes) accompanied by a decrease in mean annual precipitation of up to 20% of modern values (Webb et al. 1993). These changes are reflected in a northward and eastward expansion of prairie vegetation into now-forested regions (Webb et al. 1993). Lake-level data from eastern North America, which show that the lakes were lower than today at 6 kyr BP (Harrison 1989; Webb et al. 1993), also support the reconstruction of conditions significantly more arid than today. Pollen and lake-level based reconstructions of effective moisture suggest that conditions were drier than today in the northwest and the northern Great Basin (Thompson et al. 1993) and both drier and warmer than today in the interior plains of southern Canada (Ritchie and Harrison 1993). There is evidence for extensive aeolian activity, including reactivation of dunes and loess deposition, in the midcontinental interior sometime during the early to mid-Holocene (e.g., Muhs 1985; Muhs and Maat 1993; Maat and Johnson 1996), which is again consistent with the simulation of conditions more arid than today.

Palaeoenvironmental data from the interior of Eurasia, however, do not show conditions warmer and more arid than today. There is no evidence that steppe (warm or cool grass/shrub) expanded into regions occupied by forests today (Tarasov et al. 1998). In the region north of the Black and Caspian Seas, pollen-based biome reconstructions suggest that forest actually expanded into regions occupied today by steppe and desert (Prentice et al. 1996; Tarasov et al. 1998). This finding is consistent with lake-level data from Kazakhstan and Mongolia, which also indicate that conditions were wetter than today in the continental interior during the mid-Holocene (Harrison et al. 1996).

d. The Afro–Asian monsoon

Palaeoenvironmental data from northern Africa, central Asia, and northwestern China indicate conditions considerably wetter than today at 6 kyr BP (Street and Grove 1976; Street-Perrott and Perrott 1993; Jolly et al. 1998a; Jolly et al. 1998b; Shi et al. 1993; Winkler and Wang 1993; Yu et al. 1998) Pollen-based biome reconstructions from northern Africa (Jolly et al. 1998a; Jolly et al. 1998b) and from China (Yu et al. 1998) indicate a substantial expansion of moisture-demanding vegetation into now-arid regions of the Sahara and Inner Mongolia in response to increased precipitation due to the expansion of the Afro–Asian monsoons. Jolly et al. (1998a) indicate that the southern limit of the Sahara

was at least as far north as 23°N. None of the PMIP models simulate the observed regression of herbaceous biomes such as tundra and semidesert in Inner Mongolia. Although the PMIP simulations show a northward expansion of steppe and xerophytic biomes at the expense of desert in the Sahara, none of the models produce steppic vegetation north of ~19°N. These results confirm the results of an earlier evaluation of the PMIP simulations using lake-level data (Yu and Harrison 1996), which indicated that the PMIP simulations substantially underestimate the area affected by the enhancement of the Afro–Asian summer monsoons.

e. Equatorial aridity

There are relatively few pollen sites from equatorial Africa, and most of these lie outside the region currently occupied by tropical rain forest. However, one site (Barombi Mbo, Cameroon) that lies within the tropical rain forest today was characterized by tropical deciduous forest at 6 kyr BP (Jolly et al. 1998b) and thus supports the simulated increase in aridity in the African equatorial zone. Pollen and lake-level data from the tropical and subtropical lowlands of South America suggest that conditions at 6 kyr BP were considerably drier than today (Markgraf 1993), again consistent with the PMIP simulations. Although there are some pollen data from equatorial regions of Oceania (e.g., Markgraf et al. 1992; Hope 1996), it is currently not possible to reconstruct changes in the extent of tropical rain forest at 6 kyr BP with any reliability.

f. The Southern Hemisphere extratropics

Simulated vegetation changes in the southern extratropical zone of South America and Africa are small, and this is consistent with the pollen data from these regions (Markgraf et al. 1992; Markgraf 1993; Jolly et al. 1998a; Jolly et al. 1998b). The simulations show more significant changes in vegetation distribution across Australia, but differ on whether the continental interior becomes wetter or drier than present. The pollen and lake-level data currently available from Australia (e.g., Harrison and Dodson 1993) are mainly concentrated in coastal regions, and the reconstructions of changes in effective moisture at those few sites from the margins of the continental interior are inconclusive.

7. Discussion

The simulated response to orbital forcing in the PMIP experiments is suprisingly small compared to some earlier simulations of the 6 kyr BP climate (e.g., Kutzbach and Guetter 1986; Liao et al. 1994) and is in some key respects too small in comparison with the changes shown by palaeoenvironmental observations. Underestimation of climate change may partly be explained by the prescription of ocean and land surface conditions as modern. A simulation made with the CCM1 model coupled to a mixed layer ocean, for example, produced significant decreases in Northern Hemisphere sea ice, increased warmth in the Arctic, and somewhat larger overall changes in vegetation distribution (Kutzbach et al. 1998). This simulation yielded a global kappa value of 0.61, a value of 0.61 for the Northern Hemisphere extratropics, and of 0.54 for the intertropical zone. Similarly, experiments in which the vegetation distribution was changed to reflect observed changes in, for example, boreal forest or grassland vegetation in northern Africa at 6 kyr BP, also produced larger changes in simulated climate and biomes (TEMPO 1996; Kutzbach et al. 1996).

However, the use of prescribed (modern) ocean and land surface conditions may not provide a complete explanation for the rather small response shown in these experiments. Yu and Harrison (1996), on the basis of an analysis of the hydrological budget of five of the simulations used here (UGAMP 2.0, UKMO HADAM2, ECHAM 3.2, CCM2, LMD-LMCE 4ter), have drawn attention to the fact that the PMIP experiments show a much smaller monsoon response to orbital forcing than experiments made with an early version of the CCM (CCM0), which also had prescribed (modern) ocean and land surface conditions (Kutzbach and Guetter 1986). While this may reflect changes in the models (e.g., in the parameterization of the land surface or in the spatial resolution of the model grid), the fact that 10 different models show a rather similar magnitude of change suggests that the explanation for the smaller response may lie elsewhere.

Although the overall response to orbital forcing is small, there are nevertheless significant changes in regional climates. For example, most of the models produce a statistically significant increase in summer precipitation in the Sahel zone, and in summer temperatures along the Arctic coast. However, vegetation provides a conservative measure of climate changes because shifts from one vegetation type to another are controlled to a large extent by climatic thresholds (Woodward 1987). Climate changes that are statistically significant may still be too small to produce vegetation shifts. Thus, in evaluating paleoclimate simulations against palaeoenvironmental observations, it is important to demonstrate that the simulated climate changes are not only in the right direction but also of sufficent magnitude to produce the observed palaeoenvironmental changes. Such comparisons are facilitated by the use of process-based models of vegetation, such as BIOME, or physically based models of surface hydrology [e.g., SWAM; see Coe (1997)] to deduce simulated palaeoenvironmental changes in such a way as to allow direct comparisons with palaeoenvironmental observations.

Changes in climate in response to a change in forcing are normally expressed in terms of global and/or regional averages, because of perceived uncertainties in the reliability of simulated regional climate changes.

However, our comparisons suggest that global or zonal averages may mask the relationship between simulated climate changes and the response of the vegetation. It is only possible to derive coherent relationships between the vegetation response (as measured by kappa values) and the underlying climate changes for limited regions, such as the Sahel, where the climate changes are unidirectional. Regional patterns as shown in the biome maps thus provide a perspective on intermodel differences that is complementary to that given by large-scale averages of meteorological variables, and this perspective is necessary in order to make quantitative comparisons with palaeodata that reflect changes in vegetation or hydrology.

8. Summary and conclusions

This paper has presented the first comparison of a series of parallel climate model simulations made within the PMIP project using an equilibrium vegetation model (BIOME) as a diagnostic. The results can be summarized as follows:

1) The simulated climatic response to orbital forcing is quantitatively similar for all models.
2) The models show a similar magnitude of vegetation response at global and zonal scales.
3) The models show several common broadscale features, although the regional expression of these features varies among models. These features are
   - a northward displacement of northern forest belts in response to high-latitude warming;
   - changes in forest distribution at a regional scale, including expansion of cold deciduous forest in northern Canada and the southward extension of taiga and cool conifer forests in Siberia, reflecting the simulation of winter cooling at mid- to high latitudes;
   - expansion of warm grass/shrub vegetation in the midlatitudes in response to warmer and more arid regional climates;
   - expansion of moisture-demanding biomes and reduction in the extent of Northern Hemisphere deserts in consequence of the expanded Afro–Asian monsoon;
   - reduction of tropical rainforest as a consequence of increased equatorial aridity.
4) Comparisons with palaeoenvironmental data show that
   - the northward displacement of the northern forest belts is realistic, but the magnitude of the simulated northward shift is up to 4°–5° lat less than observed, indicating that the PMIP simulations consistently underestimate high-latitude warming;
   - the simulated winter cooling in midlatitudes is realistic for eastern North America, but biome reconstructions from southern Fennoscandia, Siberia, and China suggest that winters in these regions were considerably warmer than present; this feature is not captured by the PMIP simulations;
   - the simulation of strong midcontinental warming and aridity is consistent with the available pollen, lake, and aeolian data from North America, but palaeoenvironmental data from Eurasia show no evidence of enhanced midcontinental aridity;
   - the simulated enhancement of the Afro–Asian monsoon is realistic, but the area affected is much smaller than shown by observations; the simulated northward shift of the Sahara–Sahel boundary is at least 4°–5° lat less than observed;
   - the simulated reduction of tropical rain forest is consistent with those few observations that are available from the equatorial zone.
5) There are differences among the regional-scale vegetation changes simulated by the different models. These differences are greater for biome shifts controlled by changes in moisture budget than for those controlled by temperature.
6) The differences among model simulations in terms of vegetation distribution are not adequately reflected in global, zonal, or continental climate averages.
7) Climate changes may be statistically significant, but nevertheless insufficient to produce a discernible change in biome distribution because of the existence of thresholds in the response of vegetation to climate.

This study has established that the BIOME model is a useful tool for model intercomparisons. It has demonstrated that intermodel differences are small at a global or zonal scale, and therefore that regional-scale analyses will be necessary to identify the underlying causes of intermodel differences. Analyses of the biome maps have pinpointed some of the key regions where there are significant differences between the PMIP simulations, and which therefore merit systematic study. In some cases, these are regions where the simulated vegetation changes are in the right direction but of insufficient magnitude. In other cases, the direction of the change in vegetation differ between the models and only some of the models are capable of producing a change consistent with the observed vegetation pattern. The analyses raise methodological issues that will need to be considered in designing future PMIP experiments. Specifically, it is important to understand why the response to orbital forcing in the PMIP experiments is smaller than in previous 6 kyr BP experiments and why there are some regions where all of the models fail to capture the direction of the observed vegetation changes.

Acknowledgments. Financial support for the biome simulations was provided by the European Community (EV5V-CT95-0075), the Swedish Natural Science Research Council (G-AA/GU 09334-321), and by the Craaford Fund (‘‘The role of sea-ice and vegetation

feedbacks in the last interglacial and mid-Holocene climates of northern Eurasia''). This research is a contribution to TEMPO (Testing Earth System Models with Paleoenvironmental-Observations), the IGBP-GAIM (Global Analysis, Interpretation and Modelling) Task Force ''6000 yr BP experiment,'' and PMIP, (Paleoclimate Modelling Intercomparison Project). PMIP is sponsored by the IGBP and WCRP. We thank Colin Prentice and Jon Foley for their comments on the manuscript.

REFERENCES

Alexander, R. C., and R. L. Mobley, 1976: Monthly average sea-surface temperatures and ice-pack limits on a 1° global grid. *Mon. Wea. Rev.,* **104,** 143–148.

Anderson, P. M., and L. B. Brubaker, 1994: Vegetation history of northcentral Alaska: A mapped summary of late-Quaternary pollen data. *Quat. Sci. Rev.,* **13,** 71–92.

Bartlein, P. J., I. C. Prentice, and T. Webb III, 1986: Climatic response surfaces from pollen data for some eastern North American taxa. *J. Biogeogr.,* **13,** 35–57.

Bartman, F. L., 1980: A time variable model of Earth's albedo. NASA Grant NSG-1482, University of Michigan, 70 pp. [Available from University of Michigan, Ann Arbor, MI 48109.]

Berger, A. L., 1978: Long-term variations of caloric solar radiation resulting from the earth's orbital elements. *Quat. Res.,* **9,** 139–167.

——, and M. F. Loutre, 1991: Insolation values for the climate of the last 10 million years. *Quat. Sci. Rev.,* **10,** 297–317.

——, ——, and C. Tricot, 1993: Insolation and Earth's orbital periods. *J. Geophys. Res.,* **98,** 10 341–10 362.

Blondin, C., and H. Böttger, 1987: The surface and subsurface parameterization scheme in the ECMWF forecasting system: Revision and operational assessment of weather elements. ECMWF Tech. Memo 135, ECMWF, Reading, United Kingdom. [Available from European Centre for Medium-Range Weather Forecasts, Shinfield Park, Reading, Berkshire R62 9AX, United Kingdom.]

Bonan, G. B., 1995a: Land–atmosphere CO_2 exchange simulated by a land surface process model coupled to an atmospheric general circulation model. *J. Geophys. Res.,* **100,** 2817–2831.

——, 1995b: Sensitivity of a GCM simulation to inclusion of inland water surfaces. *J. Climate,* **8,** 2691–2704.

——, 1996: A land surface model (LSM version 1.0) for ecological, hydrological, and atmospheric studies: Technical description and user's guide. NCAR Tech. Note NCAR/TN-417-STR, NCAR, Boulder, CO, 165 pp. [Available from National Center for Atmospheric Research, P.O. Box 3000, Boulder, CO 80307.]

Budyko, M. I., 1956: *Heat Balance of the Earth's Surface.* Gidrometeozidat, 255 pp.

Choisnel, E., 1984: Un modèle agrométéorologique opérationnel de bilan hydrique utilisant des données climatiques. *Extended Abstracts, Conf. Int. CIID ''Les Besoins en Eau des Cultures,''* Paris, France.

Claussen, M., 1996: Variability of global biome patterns as function of initial and boundary conditions in a climate model. *Climate Dyn.,* **12,** 371–379.

——, 1997: Modeling bio-geophysical feedback in the African and Indian monsoon region. *Climate Dyn.,* **13,** 247–257.

——, and M. Esch, 1993: Biomes computed from simulated climatologies. *Climate Dyn.,* **9,** 235–243.

——, and V. Gaylor, 1997: The greening of Sahara during the mid-Holocene: Results of an interactive atmosphere–biosphere model. *Global Ecol. Biogeogr. Lett.,* **6,** 369–377.

Coe, M., 1997: The simulation of continental surface water: An application in Holocene North Africa. *J. Climate,* **10,** 1680–1689.

Cohen, J., 1960: A coefficient of agreement for nominal scales. *Educ. Psychol. Meas.,* **20,** 37–46.

COHMAP Members, 1988: Climatic changes of the last 18,000 years: Observations and model simulations. *Science,* **241,** 1043–1052.

de Noblet, N., I. C. Prentice, S. Joussaume, D. Texier, A. Botta, and A. Haxeltine, 1996: Possible role of atmospheric–biosphere interactions in triggering the last glaciation. *Geophys. Res. Lett.,* **23,** 3191–3194.

Ducoudré, N., K. Laval, and A. Perrier, 1993: SECHIBA, a new set of parameterizations of the hydrologic exchanges at the land–atmosphere interface within the LMD atmospheric general circulation model. *J. Climate,* **6,** 248–273.

Foley, J., J. E. Kutzbach, M. T. Coe, and S. Levis, 1994: Feedbacks between climate and boreal forests during the Holocene epoch. *Nature,* **371,** 52–54.

Gallimore, R. G., and J. E. Kutzbach, 1989: Effects of soil moisture on the sensitivity of a climate model to earth orbital forcing at 9000 yr BP. *Climate Change,* **14,** 175–205.

Gates, W. L., 1976: Modeling the Ice-Age climate. *Science,* **191,** 1138–1144.

——, 1992: AMIP: The Atmospheric Model Intercomparison Project. *Bull. Amer. Meteor. Soc.,* **73,** 1962–1970.

——, and Coauthors, 1996: Climate models—Evaluation. *Climate Change 1995: The Science of Climate Change,* J. T. Houghton, L. G. Meira Filho, B. A. Callander, N. Harris, A. Kattenberg, and K. Maskell, Eds., Cambridge University Press, 228–284.

Geleyn, J.-F., and H. J. Preuss, 1983: A new data set of satellite-derived surface albedo values for operational use at ECMWF. *Arch. Meteor. Geophys. Bioklimatol.,* **32A,** 353–359.

Gregory, D., and R. N. B. Smith, 1990: Canopy, surface and soil hydrology. UKMO Unified Model Documentation Paper 25, UKMO, Bracknell, United Kingdom, 100 pp. [Available from United Kingdom Meteorological Office, London Road, Bracknell, Berkshire RG12 2SY, United Kingdom.]

Hack, J. J., B. A. Boville, B. P. Briegleb, J. T. Kiehl, P. J. Rasch, and D. L. Williamson, 1993: Description of the NCAR Community Climate Model (CCM2). NCAR Tech. Note TN-382+STR, NCAR, Boulder, CO, 120 pp. [Available from National Center for Atmospheric Research, P. O. Box 3000, Boulder, CO 80307.]

——, ——, J. T. Kiehl, P. J. Rasch, and D. L. Williamson, 1994: Climate statistics from the National Center for Atmospheric Research community climate model CCM2. *J. Geophys. Res.,* **99,** 20 785–20 813.

Hall, N. M. J., and P. J. Valdes, 1997: A GCM simulation of the climate 6000 years ago. *J. Climate,* **10,** 3–17.

Harrison, S. P., 1989: Lake levels and climatic change in eastern North America. *Climate Dyn.,* **3,** 157–167.

——, and J. Dodson, 1993: Climates of Australia and New Guinea since 18,000 yr BP. *Global Climates since the Last Glacial Maximum,* H. E. Wright Jr., J. E. Kutzbach, T. Webb III, W. F. Ruddiman, F. A. Street-Perrott, and P. J. Bartlein, Eds., University of Minnesota Press, 265–293.

——, J. E. Kutzbach, I. C. Prentice, P. Behling, and M. T. Sykes, 1995: The reponse of Northern Hemisphere extratropical climate and vegetation to orbitally-induced changes in insolation during the last interglacial: Results of atmospheric general circulation model and biome simulations. *Quat. Res.,* **43,** 174–184.

——, G. Yu, and P. E. Tarasov, 1996: The Holocene lake-level record from Eurasia. *Quat. Res.,* **45,** 138–159.

Hewitt, C. D., and J. F. B. Mitchell, 1996: GCM simulations of the climate of 6 kyr BP: Mean changes and interdecadal variability. *J. Climate,* **9,** 3505–3529.

Hope, G., 1996: Quaternary change and the historical biogeography of Pacific islands. *The Origin and Evolution of Pacific Island Biotas, New Guinea to Eastern Polynesia: Patterns and Processes,* A. Keast, and S. E. Miller, Eds., SPB Academic Publishing, 165–190.

Imbrie, J., 1985: A theoretical framework for the Pleistocene Ice Ages. *J. Geol. Soc. (London),* **142,** 417–432.

Jolly, D., S. P. Harrison, B. Damnati, and R. Bonnefille, 1998a: Sim-

ulated climate and biomes of Africa during the late Quaternary: Comparison with pollen and lake status data. *Quat. Sci. Rev.*, **17,** 629–657.

——, and Coauthors, 1998b: Biome reconstruction from pollen and plant macrofossil data for Africa and the Arabian peninsula at 0 and 6 ka. *J. Biogeogr.*, in press.

Joussaume, S., and K. E. Taylor, 1995: Status of the Paleoclimate Modeling Intercomparison Project (PMIP). *Proc. First Int. AMIP Science Conf.*, Monterey, CA, WCRP, 425–430.

——, J. Jouzel, and R. Sadourny, 1989: Simulations of the last glacial maximum with an atmospheric general circulation model including paleoclimatic tracer cycles. *Understanding Climatic Change, Geophys. Monogr.*, No. 52, Amer. Geophys. Union, 159–162.

Kattenberg, A., and Coauthors, 1996: Climate models—Projections of future climate. *Climate Change 1995: The Science of Climate Change*, J. T. Houghton, L. G. Meira Filho, B. A. Callander, N. Harris, A. Kattenberg, and K. Maskell, Eds., Cambridge University Press, 285–357.

Kiehl, J. T., 1994: Sensitivity of a GCM climate simulation to differences in continental versus maritime cloud drop size. *J. Geophys. Res.*, **99,** 23 107–23 115.

——, B. Boville, B. Briegleb, J. Hack, P. Rasch, and D. Williamson, 1996: Description of the NCAR Community Climate Model (CCM3). NCAR Tech. Note NCAR/TN-420-STR, NCAR, Boulder, CO. [Available from National Center for Atmospheric Research, P. O. Box 3000, Boulder, CO 80307.]

Kutzbach, J. E., and B. L. Otto-Bleisner, 1982: The sensitivity of the African-Asian monsoonal climate to orbital parameter changes for 9000 years B. P. in a low-resolution general circulation model. *J. Atmos. Sci.*, **39,** 1177–1188.

——, and P. J. Guetter, 1986: The influence of changing orbital parameters and surface boundary conditions on climate simulations for the past 18 000 years. *J. Atmos. Sci.*, **43,** 1726–1759.

——, and R. G. Gallimore, 1988: Sensitivity of a coupled atmosphere/mixed layer ocean model to changes in orbital forcing at 9000 years BP. *J. Geophys. Res.*, **93,** 803–821.

——, P. J. Guetter, P. Behling, and R. Selin, 1993: Simulated climatic changes: Results of the COHMAP climate-model experiments. *Global Climates since the Last Glacial Maximum*, H. E. Wright Jr., J. E. Kutzbach, T. Webb III, W. F. Ruddiman, F. A. Street-Perrott, and P. J. Bartlein, Eds., University of Minnesota Press, 24–93.

——, G. B. Bonan, J. A. Foley, and S. P. Harrison, 1996: Feedbacks between climate and grasslands/soils in northern Africa during the middle Holocene. *Nature*, **384,** 623–626.

——, R. Gallimore, S. P. Harrison, P. Behling, R. Selin, and F. Laarif, 1998: Climate simulations for the past 21,000 years. *Quat. Sci. Rev.*, **17,** 473–506.

Lautenschlager, M., and K. Herterich, 1990: Atmospheric response to ice-age conditions: Climatology near the earth's surface. *J. Geophys. Res.*, **95** (D13), 22 547–22 557.

Leemans, R., and W. Cramer, 1991: The IIASA climate database for mean monthly values of temperature, precipitation and cloudiness on a terrestrial grid. Research Rep. RR-91-18, IIASA, Laxenburg, Austria, 62 pp. [Available from International Institute for Applied Systems Analysis, Schlossplatz 1, Laxenburg A-2361, Austria.]

Liao, X., F. A. Street-Perrott, and J. F. B. Mitchell, 1994: GCM experiments with different cloud parameterization: Comparisons with palaeoclimatic reconstructions for 6000 years B. P. *Palaeoclim.: Data Modell.*, **1,** 99–123.

Lohzkin, A. V., 1993: Geochronology of late Quaternary events in northeastern Russia. *Radiocarbon*, **35,** 429–433.

Maat, P. B., and W. C. Johnson, 1996: Thermoluminescence and new ^{14}C age estimates for late Quaternary loesses in southwestern Nebraska. *Geomorphology*, **17,** 115–128.

Manabe, S., and D. G. Hahn, 1977: Simulation of the tropical climate of an ice age. *J. Geophys. Res.*, **82,** 3889–3911.

——, and A. J. Broccoli, 1985: The influence of continental ice sheets on the climate of an ice age. *J. Geophys. Res.*, **90,** 2167–2190.

——, J. Smagorinsky, and R. F. Strickler, 1965: Simulated climatology of a general circulation model with a hydrologic cycle. *Mon. Wea. Rev.*, **93,** 769–798.

Markgraf, V., 1993: Climatic history of Central and South America since 18,000 yr B.P.: Comparison of pollen records and model simulations. *Global Climates since the Last Glacial Maximum*, H. E. Wright Jr., J. E. Kutzbach, T. Webb III, W. F. Ruddiman, F. A. Street-Perrott, and P. J. Bartlein, Eds., University of Minnesota Press, 357–385.

——, J. R. Dodson, A. P. Kershaw, M. S. McGlone, and N. Nicholls, 1992: Evolution of late Pleistocene and Holocene climates in the circum-South Pacific land areas. *Climate Dyn.*, **6,** 193–211.

Matthews, E., 1983: Global vegetation and land use: New high-resolution data bases for climate studies. *J. Climate Appl. Meteor.*, **22,** 474–487.

Mitchell, J. F. B., N. S. Grahame, and K. J. Needham, 1988: Climate simulations for 9000 years before present: Seasonal variations and effect of the Laurentide ice sheet. *J. Geophys. Res.*, **93,** 8283–8303.

Monserud, R. A., 1990: Methods for comparing global vegetation maps. Working Paper WP-90-40, IIASA, Laxenburg, Austria, 22 pp. [Available from International Institute for Applied Systems Analysis, Schlossplatz 1, Laxenburg A-2361, Austria.]

——, and R. Leemans, 1992: Comparing global vegetation maps with the Kappa statistic. *Ecol. Modell.*, **62,** 275–293.

Muhs, D. R., 1985: Age and paleoclimatic significance of Holocene sand dunes in northeastern Colorado. *Ann. Assoc. Amer. Geogr.*, **74,** 566–582.

——, and P. B. Maat, 1993: The potential response of Great Plains eolian sands to greenhouse warming and precipitation reduction. *J. Arid Environ.*, **25,** 351–361.

Overpeck, J. T., R. S. Webb, and T. Webb III, 1992: Mapping eastern North American vegetation change of the past 18 ka: No-analogs and the future. *Geology*, **20,** 1071–1074.

Peltier, W. R., 1994: Ice age paleotopography. *Science*, **265,** 195–201.

Pollard, D., and S. L. Thompson, 1995: Use of a land-surface-transfer scheme (LSX) in a global climate model: The response to doubling stomatal resistance. *Global Planet. Change*, **10,** 129–161.

Prentice, I. C., and T. Webb III, 1998: BIOME 6000: Reconstructing global mid-Holocene vegetation patterns from paleoecological records. *J. Biogeogr.*, in press.

——, W. Cramer, S. P. Harrison, R. Leemans, R. A. Monserud, and A. M. Solomon, 1992: A global biome model based on plant physiology and dominance, soil properties and climate. *J. Biogeogr.*, **19,** 117–134.

——, M. T. Sykes, M. Lautenschlager, S. P. Harrison, O. Denissenko, and P. J. Bartlein, 1994: Modelling the increase in terrestrial carbon storage after the last glacial maximum. *Global Ecol. Biogeogr. Lett.*, **3,** 67–76.

——, J. Guiot, B. Huntley, D. Jolly, and R. Cheddadi, 1996: Reconstructing biomes from palaeoecological data: A general method and its application to European pollen data at 0 and 6 ka. *Climate Dyn.*, **12,** 185–194.

Preuss, J. H., and J.-F. Geleyn, 1980: Surface albedos derived from satellite data and their impact on forecast models. *Arch. Meteor. Geophys. Bioklimatol.*, **29A,** 345–356.

Richard, P. J. H., 1995: Le couvert végétal du Québec-Labrador il y a 6000 ans BP: Essai. *Geogr. Phys. Quat.*, **49,** 117–140.

Rind, D., 1987: Components of the ice age circulation. *J. Geophys. Res.*, **92,** 4241–4281.

Ritchie, J. C., 1987: *The Postglacial Vegetation of Canada.* Cambridge University Press, 187 pp.

——, and S. P. Harrison, 1993: Western Canada—Pollen and lake level data for climatic history. *Global Climates since the Last Glacial Maximum*, H. E. Wright Jr., J. E. Kutzbach, T. Webb III, W. F. Ruddiman, F. A. Street-Perrott, and P. J. Bartlein, Eds., University of Minnesota Press, 401–414.

Shea, D. J., K. E. Trenberth, and R. W. Reynolds, 1990: A global monthly sea surface temperature climatology. NCAR Tech. Note NCAR/TN-345+STR, NCAR, Boulder, CO, 60 pp. [Available from National Center for Atmospheric Research, Boulder, CO 80307.]

Shi, Y. F., Z. C. Kong, S. M. Wang, L. Y. Tang, F. B. Wang, T. D. Yao, P. Y. Zhao, and S. H. Shi, 1993: Mid-Holocene climates and environments in China. *Global Planet. Change,* **7,** 219–233.

Street, F. A., and A. T. Grove, 1976: Environmental and climatic implications of late Quaternary lake-level fluctuations in Africa. *Nature,* **261,** 385–390.

Street-Perrott, F. A., and R. A. Perrott, 1993: Holocene vegetation, lake levels and climate of Africa. *Global Climates since the Last Glacial Maximum,* H. E. Wright Jr., J. E. Kutzbach, T. Webb III, W. F. Ruddiman, F. A. Street-Perrott, and P. J. Bartlein, Eds., University of Minnesota Press, 318–356.

——, J. F. B. Mitchell, D. S. Marchand, and J. S. Brunner, 1990: Milankovitch and albedo forcing of the tropical monsoons: A comparison of geologic evidence and numerical simulations for 9,000 yr B. P. *Trans. Roy. Soc. Edinburgh, Earth Sci.,* **81,** 407–427.

Tarasov, P. E., and Coauthors, 1998: Present-day and mid-Holocene biomes reconstructed from pollen and plant macrofossil data from the former Soviet Union and Mongolia. *J. Biogeogr.,* in press.

TEMPO, 1996: The potential role of vegetation feedbacks in the climate sensitivity of high-latitude regions: A case study at 6000 years before present. *Global Biogeochem. Cycles,* **10,** 727–736.

Texier, D., and Coauthors, 1997: Quantifying the role of biosphere–atmosphere feedbacks in climate change: A coupled model simulation for 6000 yr BP and comparison with palaeodata for northern Eurasia and northern Africa. *Climate Dyn.,* **13,** 865–881.

Thompson, R. S., C. Whitlock, P. J. Bartlein, S. P. Harrison, and W. G. Spaulding, 1993: Climatic changes in the western United States since 18,000 yr BP. *Global Climates since the Last Glacial Maximum,* H. E. Wright Jr., J. E. Kutzbach, T. Webb III, W. F. Ruddiman, F. A. Street-Perrott, and P. J. Bartlein, Eds., University of Minnesota Press, 468–513.

Thompson, S. L., and D. Pollard, 1997: Greenland and Antarctic mass balances for present and doubled atmospheric CO_2 from the GENESIS Version-2 global climate model. *J. Climate,* **10,** 871–900.

Warrilow, D. A., A. B. Sangster, and A. Slingo, 1986: Modelling of land surface processes and their influence on European climate. Dynamic Climatology Tech. Note DCTN 38, UKMO, Bracknell, United Kingdom, 23 pp. [Available from Dynamical Climatology Branch, United Kingdom Meteorological Office, London Road, Bracknell, Berkshire RG12 2SY, United Kingdom.]

Webb, T., III, P. J. Bartlein, S. P. Harrison, and K. H. Anderson, 1993: Vegetation, lake-levels, and climate in eastern North America since 12 000 yr BP. *Global Climates since the Last Glacial Maximum,* H. E. Wright Jr., J. E. Kutzbach, T. Webb III, W. F. Ruddiman, F. A. Street-Perrott, and P. J. Bartlein, Eds., University of Minnesota Press, 415–467.

Williams, J., R. G. Barry, and W. M. Washington, 1974: Simulation of the atmospheric circulation using the NCAR Global Circulation Model with Ice Age boundary conditions. *J. Appl. Meteor.,* **13,** 305–317.

Wilson, M. F., and A. Henderson-Sellers, 1985: A global archive of land cover and soils data sets for use in general circulation models. *Int. J. Climatol.,* **5,** 119–143.

Winkler, M. G., and P. K. Wang, 1993: The late-Quaternary vegetation and climate of China. *Global Climates since the Last Glacial Maximum,* H. E. Wright Jr., J. E. Kutzbach, T. Webb III, W. F. Ruddiman, F. A. Street-Perrott, and P. J. Bartlein, Eds., University of Minnesota Press, 221–261.

Woodward, F. I., 1987: *Climate and Plant Distribution.* Cambridge University Press, 174 pp.

Wright, H. E., Jr., J. E. Kutzbach, T. Webb III, W. F. Ruddiman, F. A. Street-Perrott, and P. J. Bartlein, Eds., 1993: *Global Climates since the Last Glacial Maximum.* University of Minnesota Press, 569 pp.

Yu, G., and S. P. Harrison, 1996: An evaluation of the simulated water balance of Eurasia and northern Africa at 6000 yr BP using lake status data. *Climate Dyn.,* **12,** 723–735.

——, I. C. Prentice, S. P. Harrison, and X. Sun, 1998: Biome reconstructions for China at 0 and 6ka. *J. Biogeogr.,* in press.